We are IntechOpen,
the world's leading publisher of
Open Access books
Built by scientists, for scientists

6,900
Open access books available

185,000
International authors and editors

200M
Downloads

154
Countries delivered to

Our authors are among the

TOP 1%
most cited scientists

12.2%
Contributors from top 500 universities

BOOK CITATION INDEX
CLARIVATE ANALYTICS
INDEXED

WEB OF SCIENCE™

Selection of our books indexed in the Book Citation Index
in Web of Science™ Core Collection (BKCI)

Interested in publishing with us?
Contact book.department@intechopen.com

Acoustic Emission Monitoring of Fracture Tests

Turbadrakh Chuluunbat and Andrii Kostryzhev

Additional information is available at the end of the chapter

Abstract

Identification of defect(s) where crack initiation is possible and prediction of crack propagation are of great importance in materials engineering. The current chapter analyzes the application of the acoustic emission (AE) technique for fracture monitoring in the line pipe steel during single-edge-notched tension (SENT) test and Charpy V-notch (CVN) impact test. It was found that the AE activity starts before the yield point, due to the stress concentration at the crack tip, and increases suddenly before the peak load is reached, due to the fracture initiation. Toward the end of the test, the AE hit density increases again, following intensive crack propagation. The AE analysis conducted in the present chapter showed a strong evidence of AE hit density increasing before the peak load is reached, the moment corresponding to fracture initiation.

Keywords: acoustic emission, fracture, signal analysis, tests

1. Introduction

1.1. Acoustic emission

Acoustic emission is a phenomenon whereby transient stress waves or displacement waves are generated following the rapid release of energy from localized sources such as crack initiation sites, fracture propagation, and dislocation motion in metals [1–3]. Elastic energy is transmitted through the material in the form of transient elastic waves and can be detected by sensors on the surface of a specimen (**Figure 1**).

The sensor used in AE measurements converts elastic waves into electrical signals which are then processed and analyzed by special hardware and software. Useful AE signals need to be distinguished from the background noise generated from the surroundings [4, 5]. **Figure 2** shows typical acoustic emission signal types. There are two main types of useful AE signal:
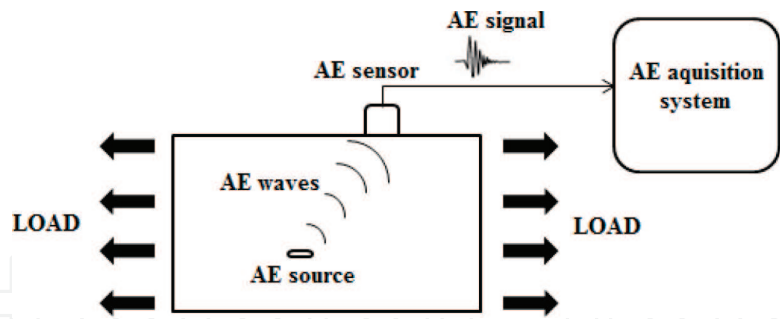
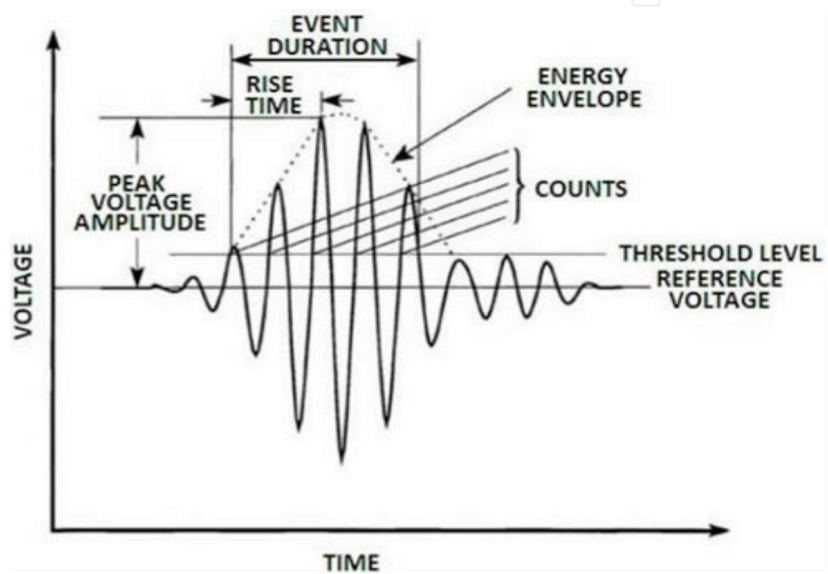**Figure 1.** Schematic presentation of AE monitoring technique.

Figure 2. Parameters of an AE hit [6].

"burst" and "continuous" [7]. Burst AE signals correspond to individual events such as stages of crack growth, brittle fracture, and impact. Continuous AE signals correspond to sustained signals generated by time-overlapping events such as plastic deformation, friction, and liquid leaks [3, 8]. It has been demonstrated that continuous low-amplitude AE signals are generated from low-energy sources. Discrete high-amplitude AE signals are generated from high-energy sources [9].

Currently, the AE technique is used in many industries for nondestructive testing of various materials and structures. A major advantage of AE measurement is that it can monitor in real time the development of defects occurring inside a material without further damaging of the material [10, 11]. However, for some applications, the operating environments are often very noisy, while the AE signals are usually very weak. This makes the detection of AE signal a challenging task.

1.2. AE source and AE signal analysis

There are two approaches to analyze AE signals: "Parameter-based" and "Waveform-based" [2]. Several AE parameters, such as oscillation count, amplitude, energy, event duration, and

rise time, can be derived from the AE signal. The major parameters used in the parameter-based analysis of the AE signal are shown in **Figure 2**.

The AE waveform and frequency analysis are usually carried out using fast Fourier transform and wavelet transform [4, 12, 13]. Identification of the AE signal can be based on the type of AE waveform and its frequency range: burst-type signal for individual events and continuous signal for prolonged events [3]. For example, the AE analysis during the fatigue cracking [13] showed three types of waveforms (**Figure 3**): from fatigue cracking (a) and (b); fretting (c) and (d); and noise (e) and (f). The microcrack (a) and (b) had strong high-frequency components above 0.5 MHz in comparison with fretting and noise, although peak amplitude was generally low.

Generally, an AE signal in metals is generated upon the initiation and growth of cracks, due to slip and dislocation movements, twinning, or phase transformation. In these cases, stress plays an important role in giving rise to AE. Plastic deformation is induced by permanent changes in the positions of atoms. These changes are related to and based on the movement of the dislocations [14]. In addition, fracture occurs when the material breaks and new surfaces are produced.

Figure 4 presents the AE sources in steel. The major macroscopic AE sources in steel are crack jumps, development of plastic deformation, fracturing and debonding of hard inclusions. The main microscopic AE sources include dislocation movement, interaction, annihilation, slip
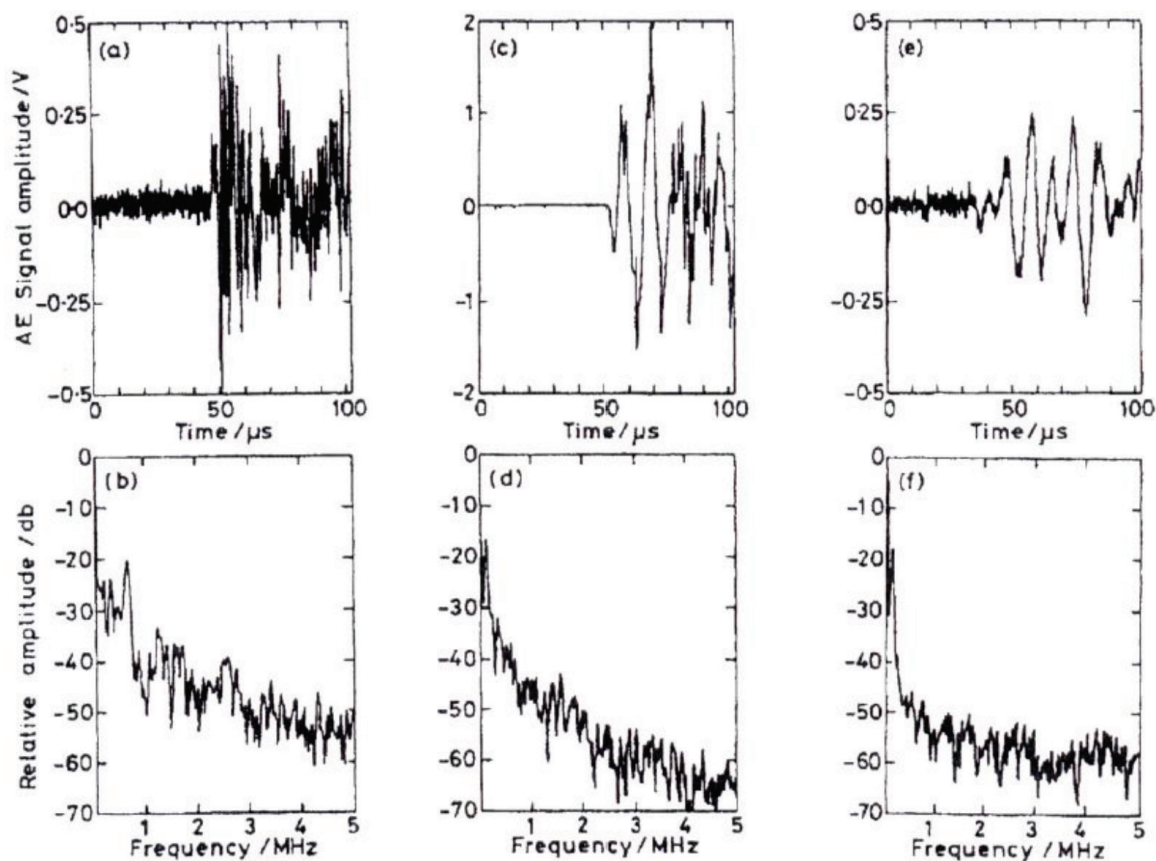

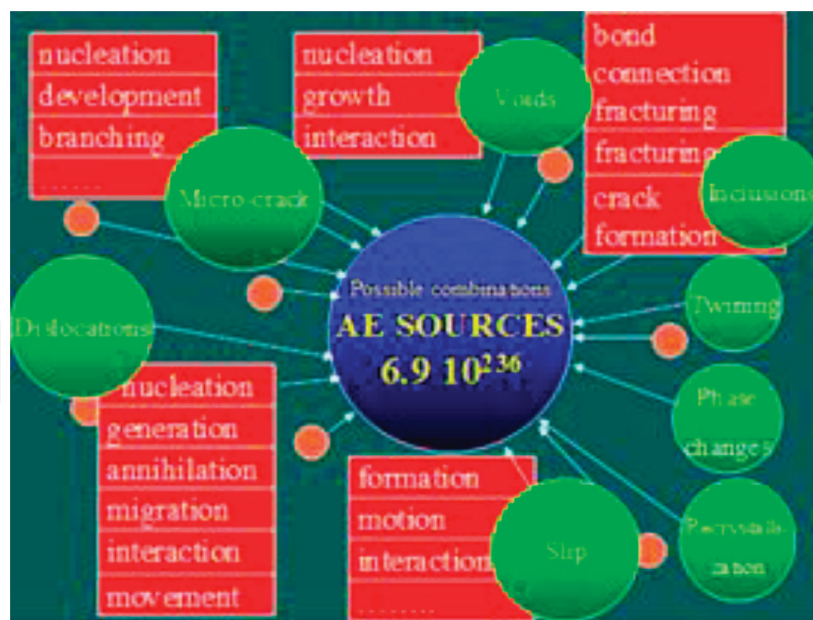**Figure 3.** Waveforms and corresponding frequency spectra [13].

Figure 4. AE sources in steel micro and macrostructure [10].

formation, void nucleation, void growth, and void interaction [15–17]. The most detectable AE signals are generated when a loaded material undergoes plastic deformation or when a material is loaded at or near its yield stress [18]. AE activity can also be observed when the material ahead of the crack tip undergoes plastic deformation (microyielding). In primary emissions arising from crack growth, there are two sources of cracks that affect the AE [19]. In the first case, there may be emissive particles (e.g., nonmetallic inclusions) in the stress concentration region near the crack tip. Since these particles are less ductile than the surrounding material, they tend to break more easily when strained. The second AE source is the propagation of crack tip occurring as a result of dislocation motion and small-scale cleavage produced by tri-axial stresses.

1.3. AE monitoring of fracture

A number of AE studies performed during tensile testing detected a burst AE signal near yielding [13], AE activity originating from movement of dislocations [20], and AE wave parameters arising from macroyielding [21]. Researchers have also studied the relationship between AE features (signal amplitude, frequency, energy, duration, and count) and test parameters (load, stress, and crack growth) during tensile testing of notched and plain metal specimens [22–27].

As can be seen from **Figure 5**, the tensile process could be divided into four stages: (1) microplastic deformation, (2) yielding, (3) strain hardening, and (4) necking and fracture. Significant AE energy release is expended in the first and second stages. AE energy decreased in stage 3, and the density of AE hits increased at stage 4 due to the occurrence of specimen fracture [20, 29].

Fracture tests were carried out to detect AE signals associated with crack initiations [27, 28, 30] and crack growth in metals [29, 31–33].
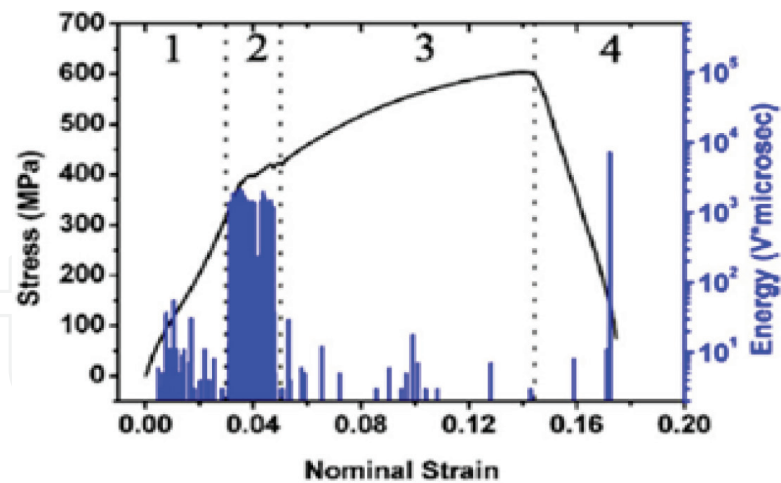
Figure 5. Stress-strain curve coupled with AE energy for tensile testing of Q345 steel [28].
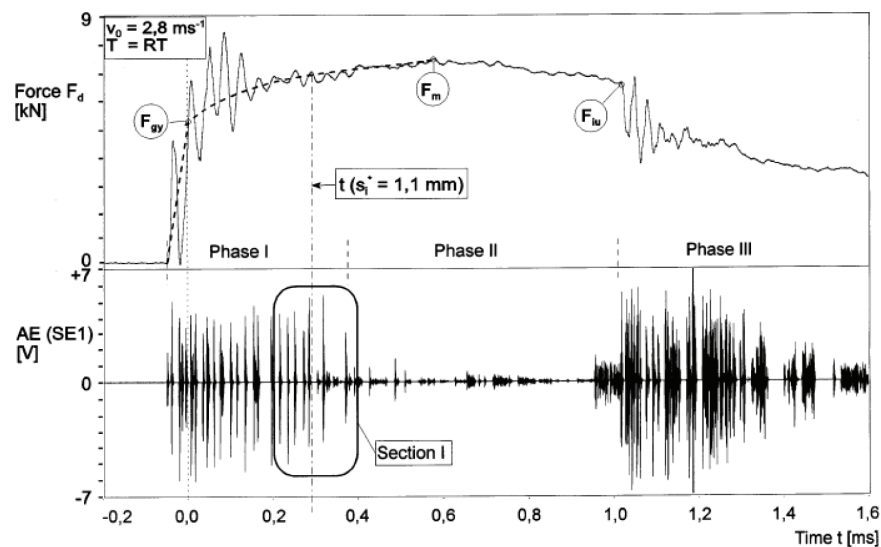

Figure 6. Load and AE signal from instrumented three point impact loading [34].

In other studies by Richter et al. [34] and [35], modified CVN specimens of 10CrMo9 steel with 20% side grooves were used to detect the onset of tearing. They did a dynamic three-point bending test using AE sensor located inside the hammer of tester (**Figure 6**).

This study investigated dynamic fracture behavior and determination of fracture initiation using the AE method. The main purpose of the investigation was to use the dynamic J integral (Jid) at crack initiation and dynamic yield stress (Gyd) for the characterization of elastic-plastic material behavior under rapid loading (impact).

Tronskar et al. [35] applied a different approach to determine the onset ductile tearing in instrumented Charpy testing of NVE 36 steel. A linear correlation was found between the time of ductile fracture initiation determined by the AE monitoring and direct displacement interferometric strip method.
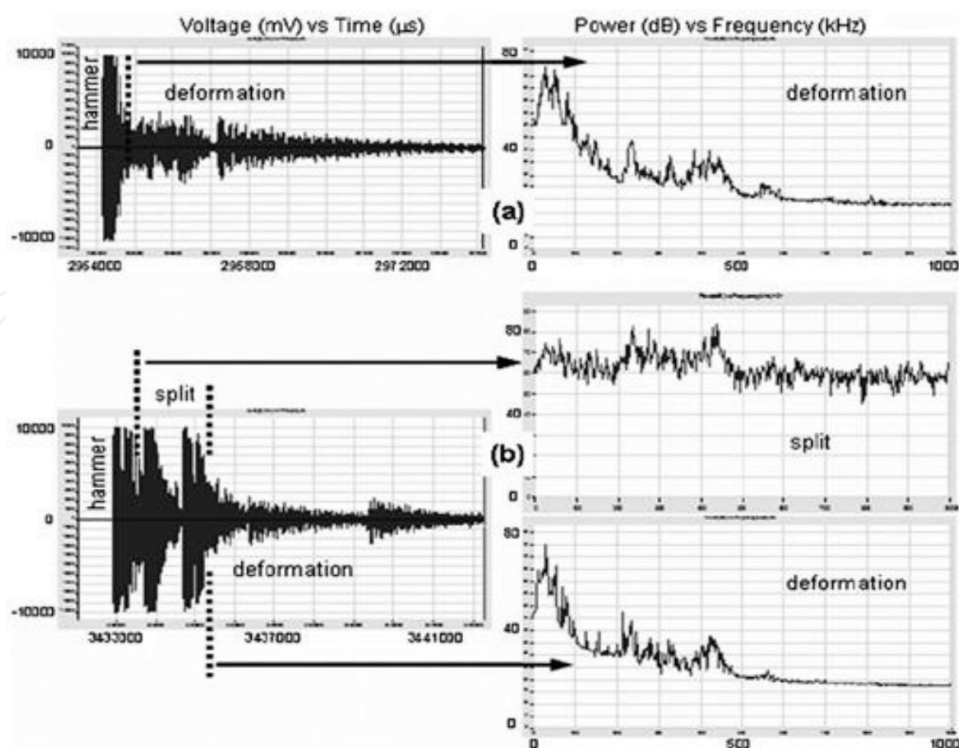
Figure 7. Acoustic emission during CVN at 60 and 80 J impact energies [12].

The possibility of detection of split formation during low-blow Charpy impact (40–100 J) testing was also shown for high-strength steel by Kostryzhev et al. [12]. AE waveform analysis was carried out to separate signals generated from the hammer, plastic deformation, and split initiation. **Figure 7** shows acoustic waves and power spectra for testing of strip steel at 60 and 80 J impact energies. The AE waves generated from crack initiation and growth were in two peak frequencies between 200 and 500 kHz and 500 and 1000 kHz. It is indicated by a shorter duration of the fracture process than that of deformation by dislocation slip.

2. Materials, equipment, and method

2.1. Materials and equipment

Two grades of pipeline steels, API-X70 and API-X80, were used in this study. Their chemical compositions are shown in **Tables 1** and **2**. All X70 specimens used in SENT and CVN tests were cut from a pipe with 14.1 mm wall thickness and 1067 mm diameter. All X80 specimens were prepared from a pipe with 25 mm wall thickness and 1067 mm diameter.

The SENT tests were carried out using an Instron 8801 servo hydraulic dynamic testing machine. The machine has console software which provides full system control from a computer including waveform generation, calibration, limit setup, and status monitoring. The testing system includes up to a 100 kN axial force capacity, a Dynacell load cell, standard height frame options, and a wide range of grips, fixtures, and accessories [36].

C	Mn	Si	Nb	Ti	V	Ni	Cr
0.0499	1.56	0.238	0.0576	0.0088	0.0256	0.214	0.028
Cu	Mo	Al	Ca	N	S	P	B
0.163	0.148	0.035	0.0015	0.0036	0.0014	0.0059	0.0001

Table 1. Composition of X70 pipeline steel (wt%).

C	Si	Mn	P	S	Cu	Alt	Nb	Ni	Cr	Ti	Ceq	Pcm
0.064	0.22	1.72	0.006	0.002	0.23	0.027	0.068	0.206	0.22	0.0158	0.42	0.18

Table 2. Composition of X80 pipeline steel (wt%).

The CVN impact tests were carried out using a 450MPX instrumented Instron Impact tester. The capacity of this machine is 750 J. The specimen temperature was controlled by a cooler containing methanol (for above −80°C) and a mixture of liquid nitrogen and methanol (for below −80°C). **Figure 8** shows the AE signal processor, manufactured by the Physical Acoustics Corporation (USA). The system consisted of a wideband sensor with an operating frequency range of 50–1000 kHz and temperature range of −65°C … + 175°C, a single-channel AE digital signal processor with an internal low noise preamplifier and a computer. The AE signal was recorded and analyzed using the AEwin software. This software has the ability to analyze waveforms and conduct fast Fourier transform (FFT). All data are saved in standard Physical Acoustics Corporation (PAC) defined DTA files.

2.2. SENT test

The geometry of a SENT specimen is conforming to DNV RP F108 specifications [37]: 12 mm in width, 6 mm in thickness, and 60 mm in gauge length. A notch representing an initial "crack" of 2 mm length and 0.3 mm width was cut using wire cutting. The crack (notch) depth

Figure 8. A single-channel AE digital signal processor.

was a third of the specimen thickness. The tests adopted a slower strain rate of 2.7×10^{-4} and a higher strain rate of 5.5×10^{-3}. **Table 3** shows testing conditions.

Additional test was conducted at a lower temperature of −20°C, while other tests were performed at room temperature (~20°C). The materials used in SENT tests were X70 and X80 line pipe steels. X70 specimens were cut using wire cutting from a 14 mm wall thickness and 1067 mm diameter pipe. X80 specimens were cut from a 25 mm wall thickness and 1067 mm diameter pipe.

A scheme of the SENT test setup is illustrated in **Figure 9**. During testing, the AE sensor was attached to the specimen using a sticky band with ultrasound treatment gel applied between the specimen and sensor surfaces as a coupling material to increase the signal quality. All the recorded waveforms were analyzed in time and frequency domain (frequency spectrum) using FFT. The crack propagation during SENT testing was observed using a MotionPro X3 high-speed camera with excellent resolution, up to 8500 µs exposure time and up to 300 of frame/sec recording rate. After testing, the fracture surface was observed by JEOL JSM-6490LA scanning electron microscope (SEM) operating at 20kV.

2.3. CVN test

The CVN test involves striking the specimen with a striker (hammer), mounted at the end of a pendulum. The CVN test procedures and specimen dimensions can be taken from the

Test number	Material grade	Temperature	Strain rate
1	X70	RT (20°C)	2.7×10^{-4}
2	X70	RT (20°C)	5.5×10^{-3}
3	X80	RT (20°C)	2.7×10^{-4}

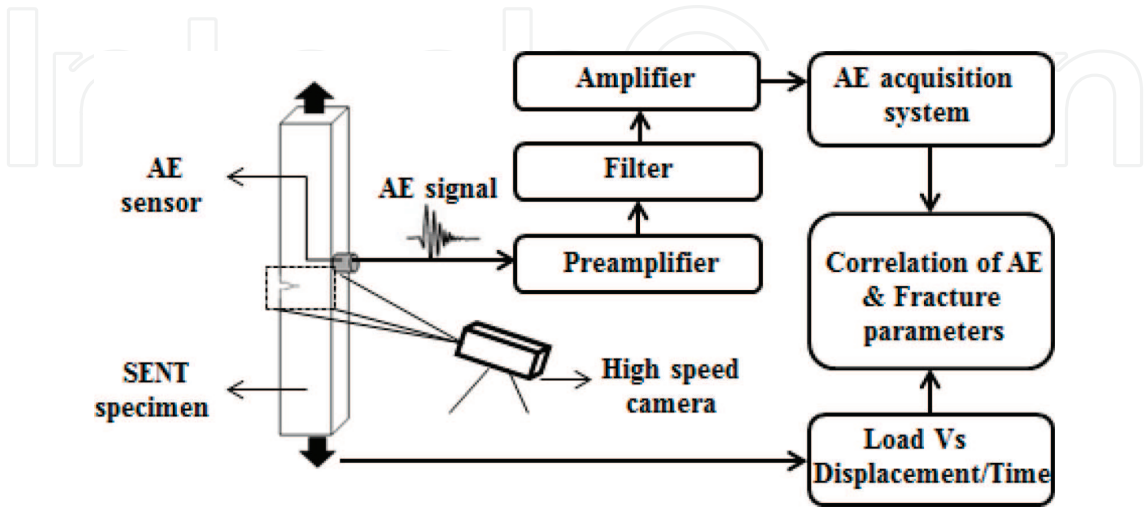**Table 3.** SENT test conditions.

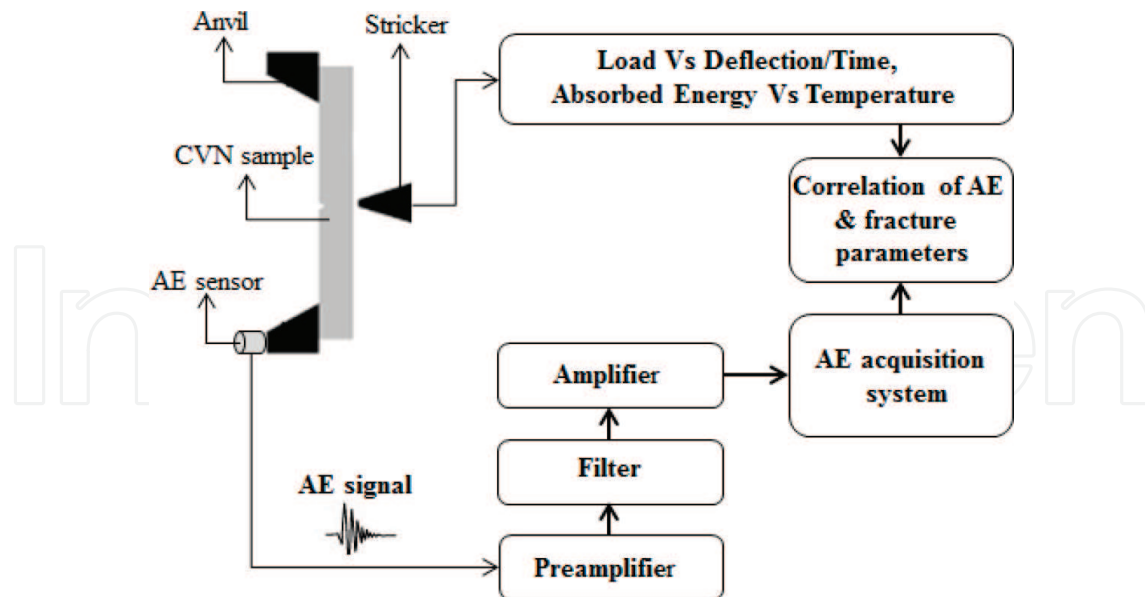**Figure 9.** A schematic of AE measurement setup of SENT testing.

Figure 10. A scheme of experimental setup for AE monitoring of Charpy testing.

Australian standard-1544.2 [38]. A scheme of the CVN test setup is illustrated in **Figure 10**. The specimen that fits in the Charpy impact tester is rectangular with a notch cut on one side. The notch represents a predetermined crack initiation location. Charpy specimens, in particular the notches, are carefully designed and prepared, since variations in notch dimensions will seriously affect the results of the tests. In this work, CVN tests using full size specimens with 10 mm thickness were performed at various temperatures: RT (20°C), −20, −40, −60, −80, −100, and − 120°C, using an instrumented Charpy impact machine. In addition, sub-size specimens with B = 5 mm and 7.5 mm were used for testing at ambient temperature. Each test has been repeated three times. During the test, the absorbed impact energy and the load-deflection curve were recorded. Before testing, specimens were kept in the cooler for at least 40 minutes to achieve a uniform temperature. The AE sensor was nonpermanently attached to one of the anvils of Charpy machine with a sticky band, and ultrasound treatment gel was applied as a coupling material to increase the signal quality. The choice for the sensor location was determined by minimizing the saturation condition.

3. Results and discussion

3.1. AE monitoring of SENT

Pipelines can be subjected to severe deformations. Local defects may result from bending, generated by ground/soil movement or washout during installation and operation, and biaxial loading, originating from longitudinal straining and internal pressure [39, 40].

To fully explain pipeline failure, research is needed to develop a better understanding of the mechanical properties and fracture behavior (initiation and propagation) in both traditional
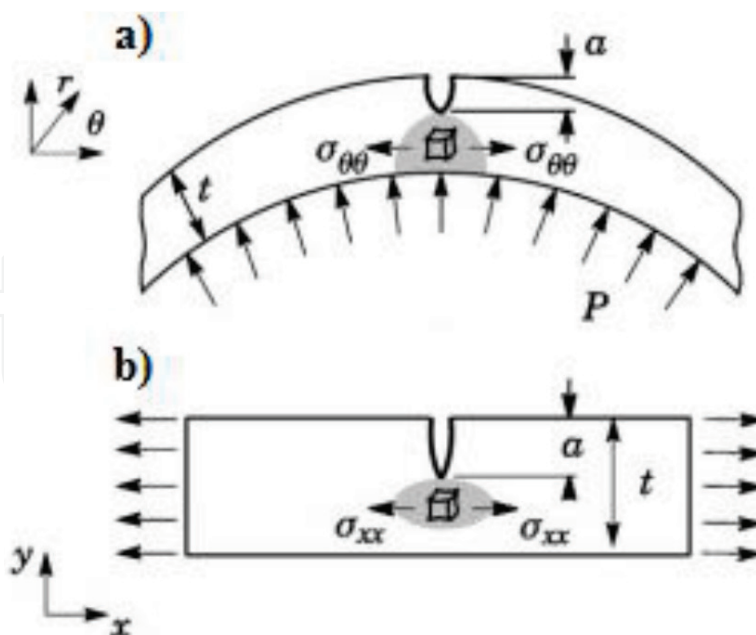
Figure 11. (a) Schematic loading condition for a pressured pipe; (b) SENT test specimen [38].

and newly developed pipeline steels. One of the representative specimens used to evaluate the fracture characteristics of the pipeline steel was designed to be compatible with a SENT test. The fracture toughness data obtained from a SENT test can be more suitable for fracture predictions of pressurized pipelines and cylindrical vessels than data obtained from notched fracture specimens under bending or impact loading [40] (**Figure 11**).

Based on the AE activity, the load-displacement curve for slow strain rate can be divided into three regions (**Figure 12**):

- Region I. There were few hits in this region with a maximum amplitude of 45 dB and average frequency varying from 80 to 100 kHz;

- Region II. The AE activity increased compared to Region I. There are seven hits in this region. The maximum amplitude is 70 dB and the average frequency ranges from 100 to 350 kHz;

- Region III. The AE activity is stable in accordance with the monotonous crack propagation. At the end of this region, the AE hit density increased significantly following the occurrence of multiple fracture events prior to separation of the specimen in two parts. The main AE signals observed in this region were of 75 dB amplitude and 200–400 kHz average frequency.

The load-displacement curve coupled with AE activity for SENT of X80 steel (**Figure 13**) has shown a higher hit density compared to X70 steel tested at the same conditions (**Figure 12**):

- Region I. There were six hits observed. The maximum amplitude was 60 dB and the average frequency varied from 50 to 150 kHz;

- Region II. The AE activity decreased compared to Region I. There were two hits in this region. The maximum amplitude was 65 dB, and the average frequency ranged from 100 to 300 kHz.

- Region III. The AE activity was relatively stable due to the monotonous crack propagation. The main AE signals observed in this region were of 80 dB amplitude and 100–300 kHz average frequency.

3.2. AE monitoring of CVN

3.2.1. Effect of specimen thickness

Figure 14 shows the load-deflection curves obtained during the CVN testing of three specimens with different thicknesses (B = 10, 7.5, and 5 mm) at ambient temperature. Three curves have similar shape, although the load increases with the specimen thickness.

All the specimens exhibited ductile fracture behavior. **Table 4** lists the CVN energy, the load at yield, and the maximum load for three specimens with different thicknesses. As the specimen thickness decreases from 10 to 5.0 mm, the CVN energy decreased from 303.3 to 108.0 J.

In this study, the AE monitoring technique was used to investigate the effect of Charpy specimen thicknesses for the first time. The AE waveforms for 5 mm specimen is shown in **Figure 15**, and the signal parameters for 5 and 7.5 mm thickness are listed in **Table 5**.

It can be found that as the specimen thickness decreases from 7.5 to 5 mm, in Region I, AE signal amplitude decreases from 10 to 8 V, and the average frequency is quite low in the range of 50–100 kHz due to the hammer impact and general yielding. In Region II, a burst AE signal is generated due to the ductile fracture initiation. Amplitude value is in the range of 4–6 V, and
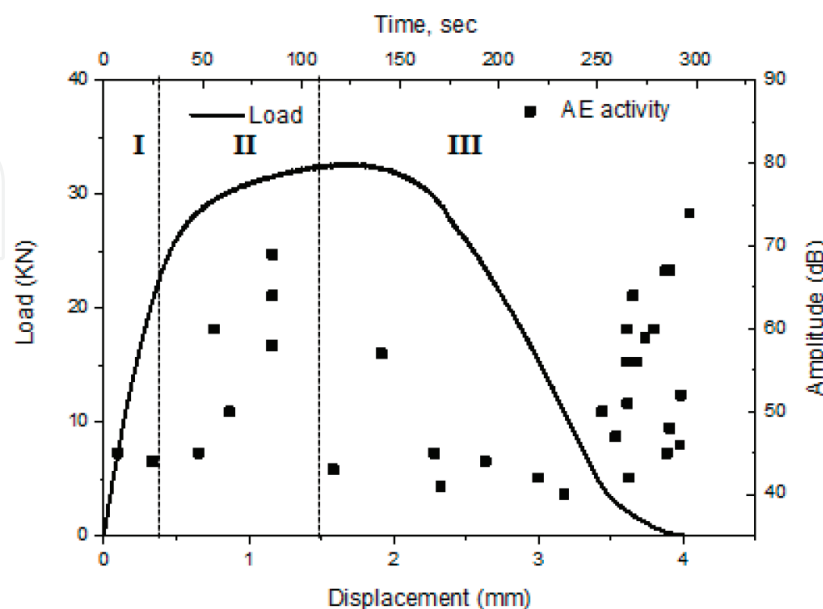

Figure 12. The load-displacement curve and AE activity for X70 steel tested at $2.7 \times 10^{-4}\ \mathrm{s}^{-1}$.

the average frequency decreased from 200 to 100 kHz. In Region III, continuous AE signals were observed due to the slightly (slowly) dropped load. The AE amplitude decreased from 8 to 4 V, and the average frequency decreased from 150 to 50 kHz.
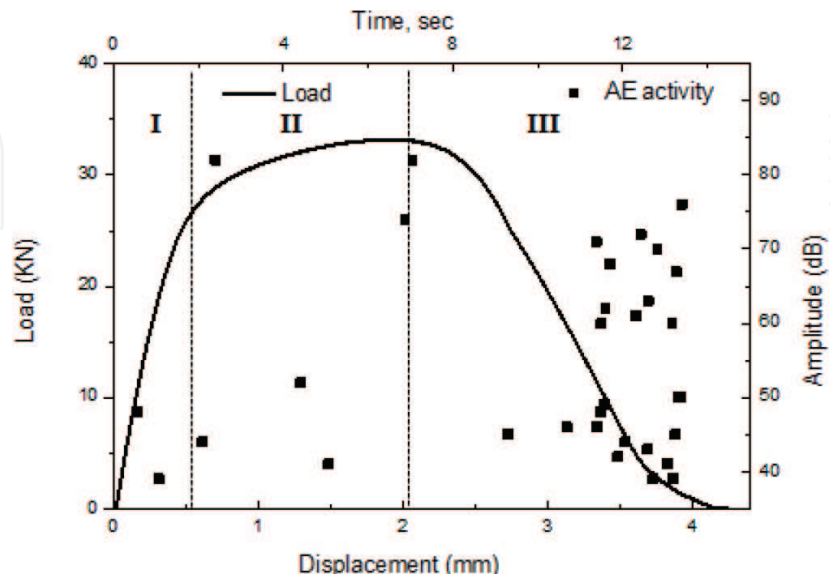

Figure 13. The load-displacement curve and AE activity for X80 steel tested at 2.7×10^{-4} s^{-1}.
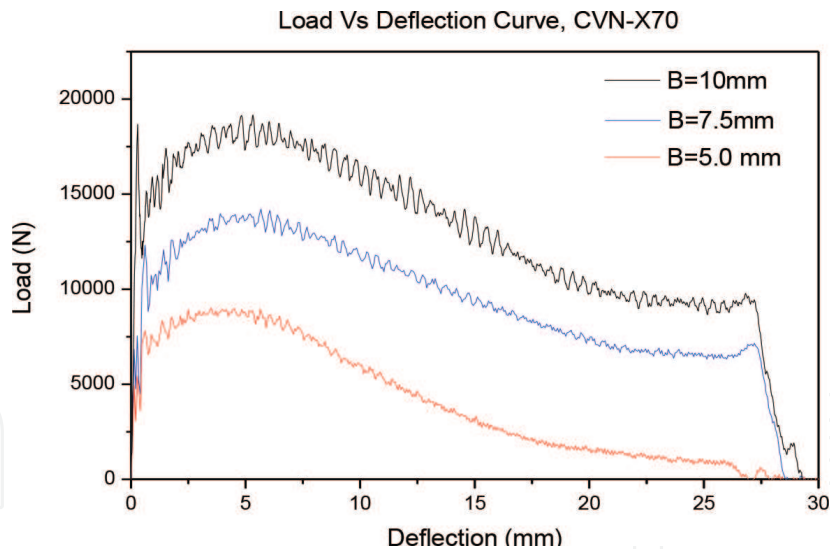

Figure 14. Load-deflection curves obtained during instrumented CVN impact testing at ambient temperature of specimens with various thicknesses.

Specimen thickness, mm	Average CVN energy, J	Load at yield, N	Maximum load, N
10	330.3	14,895	17,990
7.5	197.3	11,150	12,800
5.0	108.0	4810	6105

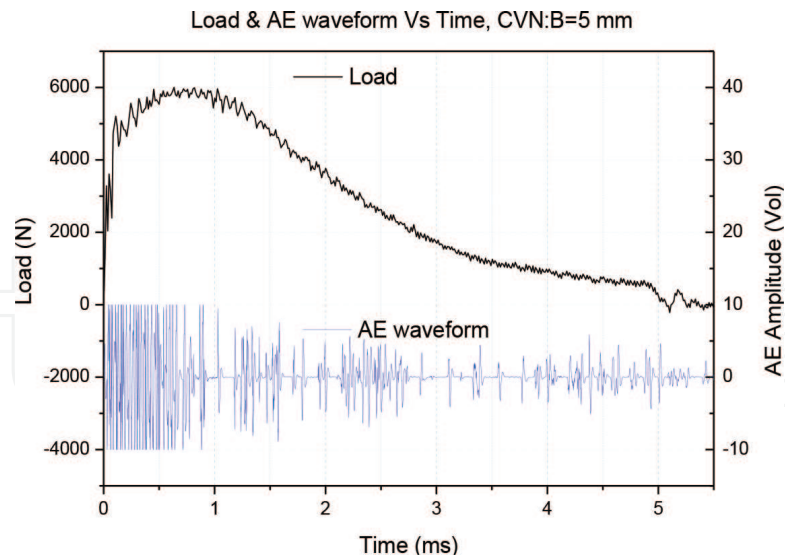**Table 4.** Experimental results for testing at ambient temperature.

Figure 15. Load and acoustic emission waves versus time for CVN impact test at ambient temperature of 5-mm specimen.

Sample thickness	Region	Amplitude, V	FFT power spectrum frequency peak, kHz	Suggested cause of AE
5.0 mm	I	<6	50–80	The hammer impact and general yielding (A)
	II	4–6	~100	Plastic deformation and ductile fracture (A–B)
	III	2–4	80–100	Ductile fracture propagation (B–C)
7.5 mm	I	<6	75–100	The hammer impact and general yielding (A)
	II	4–6	~150	Plastic deformation and ductile fracture (A–B)
	III	2–4	100–150	Ductile fracture propagation (B–C)

Table 5. The AE waveform parameters during CVN impact test in the studied X70 steel at various thicknesses.

3.2.2. Effect of temperature

Full-size CVN tests have been conducted at seven temperatures. Three representative load-deflection curves are shown in **Figure 16**.

As can be seen in **Figure 16** for 20°C, at the beginning, the load increases with the deflection. At a deflection of 5 mm, the load reaches its maximum and then gradually decreases with deflection. At the final stage of test at a deflection of around 25 mm, the load still remains at quite high value, followed by a quick drop. This behavior is due to the fact that the material is too tough to be fully broken at this temperature.

For the test at −60°C, the maximum load is higher than for 20°C. However, beyond the peak point, the drop of the load at −60°C is much faster than that for 20°C. This indicates a more brittle fracture at −60°C than at 20°C. At the final stage of −60°C test, the load gradually
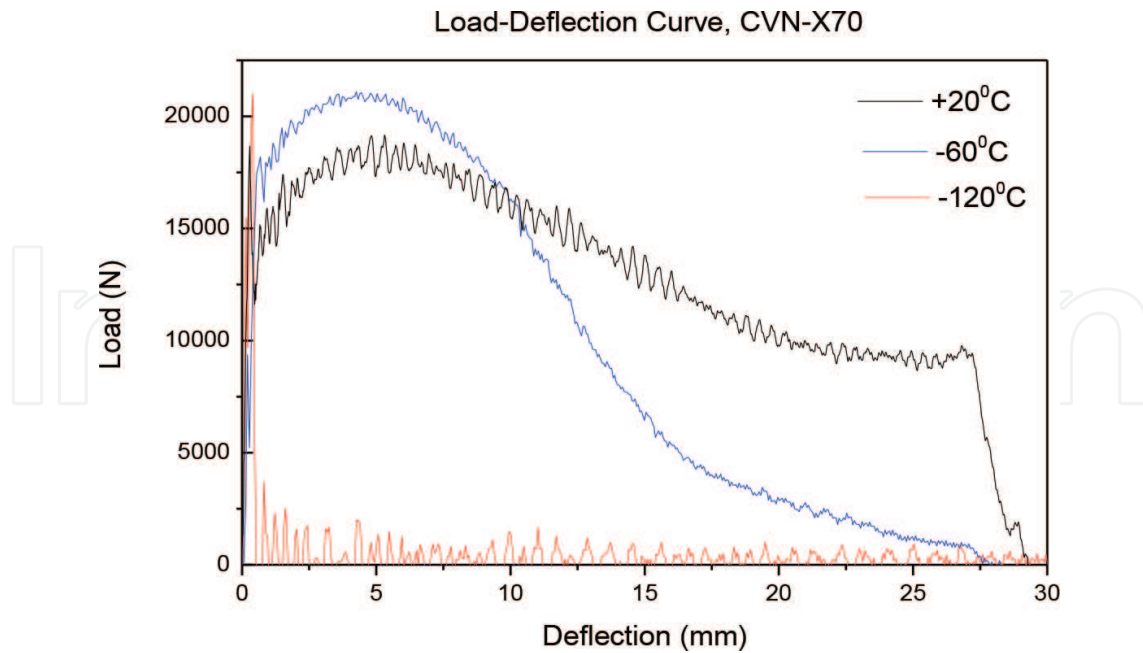
Figure 16. Load-deflection curves of instrumented Charpy impact tests at +20, −60, and − 120°C.

approaches zero. The load for −120°C test temperature reaches its maximum value at a very low defection (around 1 mm) and then rapidly drops to near zero. This clearly indicates brittle fracture mode at this temperature.

It can be seen in **Figure 17**, the fracture surface of the CVN specimen fractured at 20°C is fully ductile with 100% fibrosity. Apparent necking and shear lip areas can be seen. The region close to the notch shows a typical ductile fracture with elongated shearing dimples and micro-voids. The region far from notch also shows ductile fracture, but the dimples are much larger
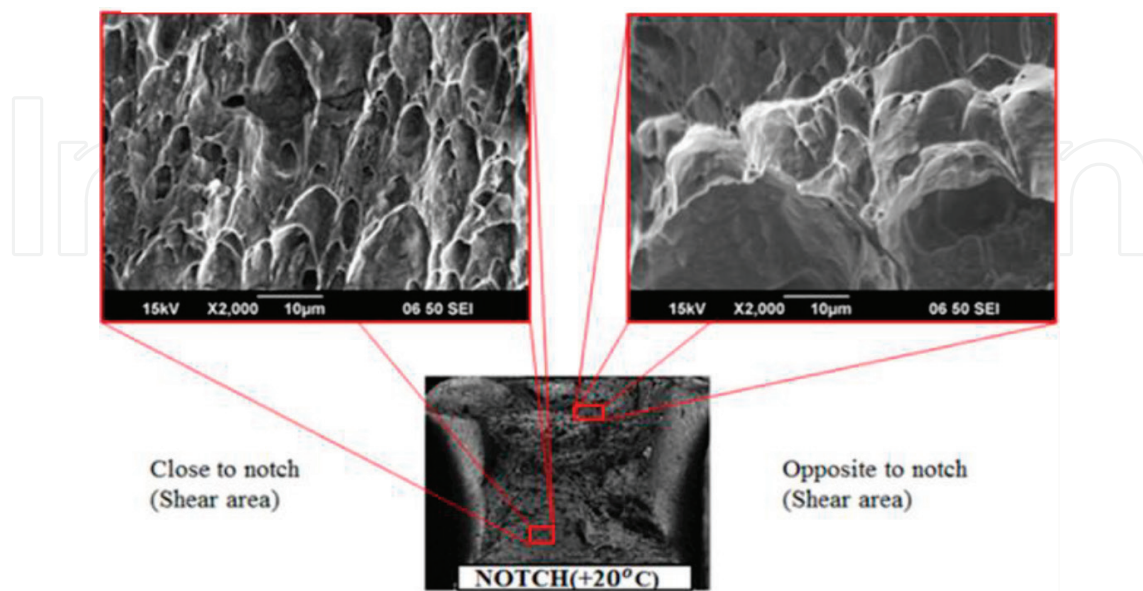

Figure 17. Fracture surface for 10-mm thick CVN specimen tested at +20°C.

in size and much shallower compared to the region close to the notch. The mechanism of ductile crack growth can be characterized by microvoid nucleation, growth, and coalescence. As a specimen is loaded, local strains and stresses at the crack tip support void nucleation. These voids grow as the crack tip blunts and link with the main crack.

The specimen fractured at −60°C shows a half ductile and half brittle type of fracture surface, as can be seen in **Figure 18**. The half close to the notch shows a similar appearance to that of **Figure 18**, with necking, shear lips, elongated dimples, and microvoids. The half close to the final fracture area shows a typical brittle fracture appearance without necking and cleavage facets are observed at high magnification.

AE waves along with the load-time curve for CVN test at −60°C are shown in **Figure 19**. For the AE signal analysis, the load-time curve was divided into three regions: I—before the yield point, II—between the yield point and the peak point, and III—after the peak point till the final fracture.

The general trends are as follows:

- Region I. A high amplitude AE signal is generated from the hammer impact and sample yielding due to a sudden increase in load under elastic condition;

- Region II. A characteristic high-frequency burst in the AE signal is observed. This corresponds to ductile fracture initiation. The phenomenon is observed for a short time between the yield point and the point of maximum load.

- Region III. AE signals generated from fracture propagation are observed. They are of a burst type at high frequency and a continuous type at frequency lower than in Region II; before the end of test, a distinct drop in load was observed that generated a high-frequency burst signal due to the occurrence of brittle fracture.
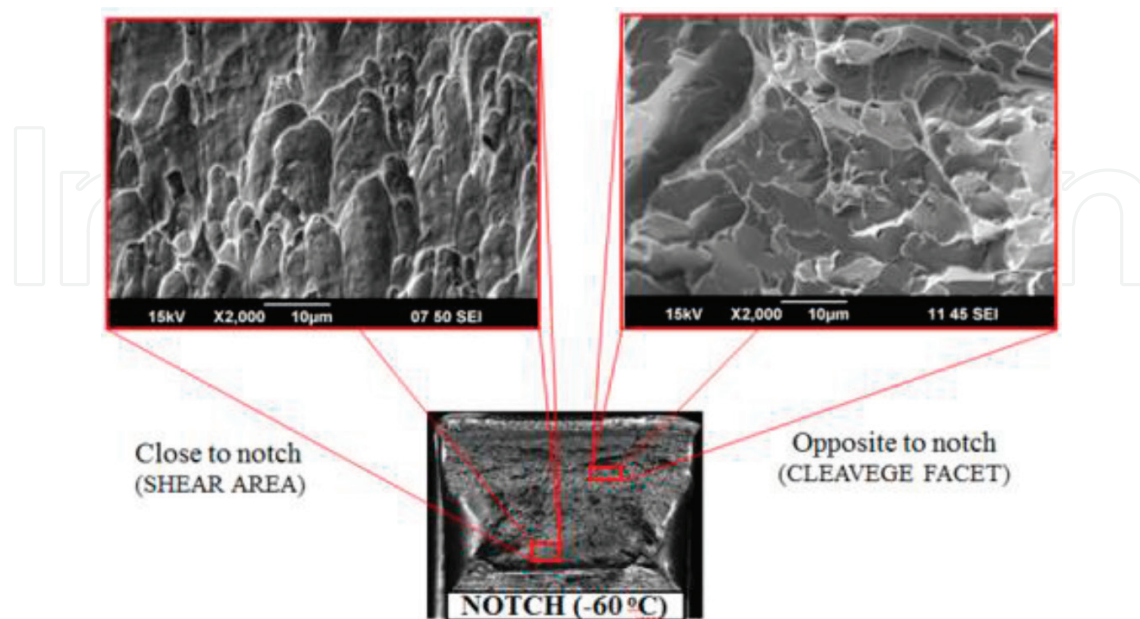

Figure 18. Fracture surface for 10-mm thick CVN specimen tested at −60°C.
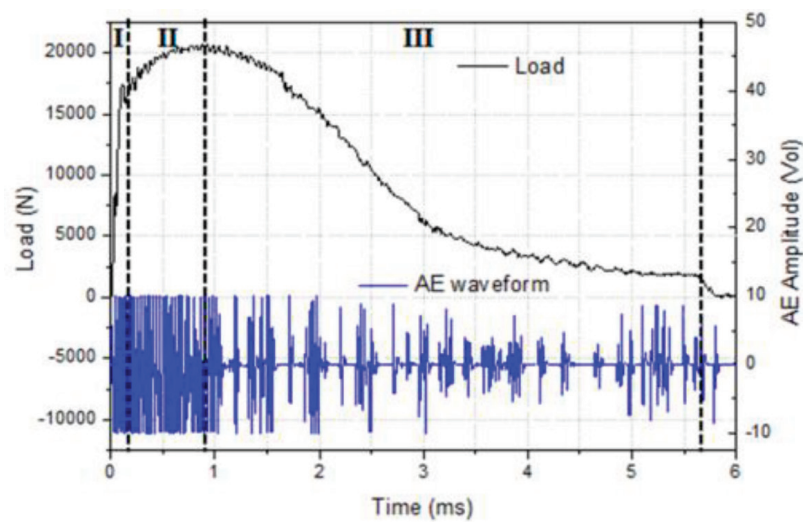
Figure 19. Load-time curve and acoustic emission wave for CVN test at −60°C temperature (B = 10 mm).

Table 6 lists the amplitude and average frequency ranges for each of three regions of the two tests conducted. With a decrease in temperature from ambient to −60°C, the AE average frequency in Region I increased from 50 to 100 kHz. In Region II, strong AE bursts were generated from crack initiation. The AE average frequency increased from 100–200 to 200–250 kHz with a decrease in test temperature. In Region III, the continuous AE signal was related to crack propagation. Although the burst signals dominated due to brittle fracture mode, amplitude increased from 4–6 to 6–8 V and the average frequency increased from 50–100 to 250–350 kHz with a decrease in temperature.

3.2.3. Investigation of fracture initiation

It has been observed by the high-speed camera and AE monitoring of the SENT tests that the fracture does not initiate at the peak load, and it always occurs between the yield point and the peak point, with higher AE amplitude and frequency associated with fracture initiation.

Testing temperature	Region	Amplitude, V	Frequency peak, kHz	Suggested cause of AE
+20°C	I	<8	50–75	The hammer impact and general yielding (A point)
	II	<4–6	100–200	Plastic deformation and ductile fracture (A–B point)
	III	>4	50–150	Ductile fracture propagation (B–C point)
−60°C	I	<8	100–150	The hammer impact and general yielding (A)
	II	4–6	200–250	Ductile fracture and crack propagation (A–B)
	III	6–8	250–350	Brittle fracture (B–C)

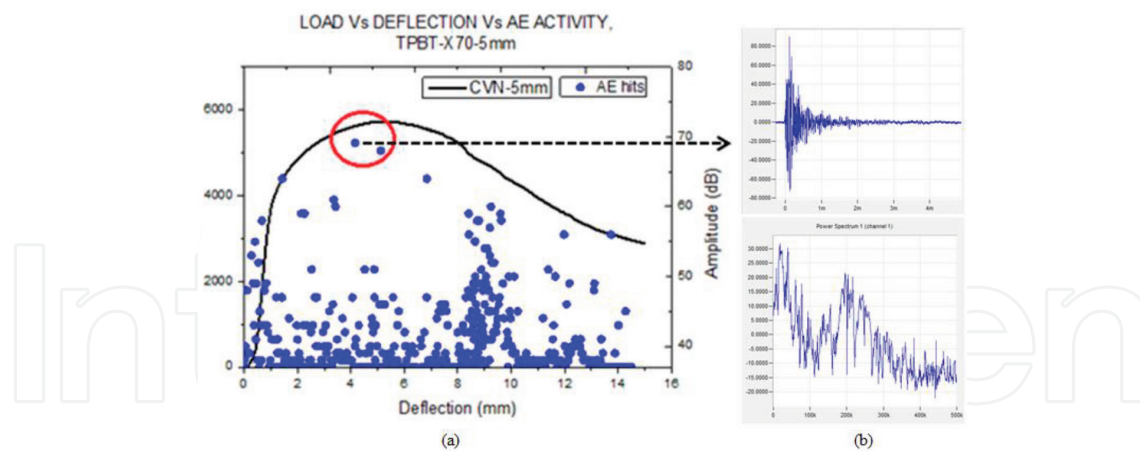**Table 6.** AE waveform parameters during CVN testing.

Figure 20. (a) AE activity corresponding to the load-deflection curve obtained during TPBT; (b) selected AE signal waveform and power spectrum corresponding to the fracture initiation for 5-mm thick CVN sample.
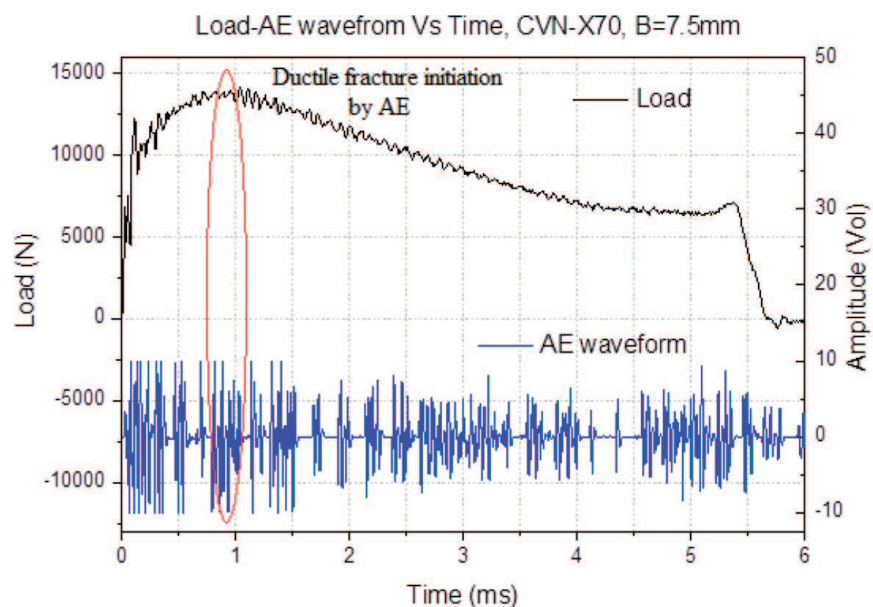

Figure 21. Load-time curve and AE wave for CVN specimen tested at RT, B = 7.5 mm.

In order to further validate the location of fracture initiation, quasi-static three point bending tests (TPBTs) were performed using a tensile test machine.

Figure 20(a) shows the load-deflection curve of the X70 line pipe steel obtained during the TPBT and corresponding AE hit amplitude distribution. It has been found that before the peak load was reached, a strong AE burst with larger amplitude, marked by a circle in the figure, was generated. High-speed video indicated that the fracture initiation was responsible for this AE burst event. **Figure 20(b)** shows this hit waveform and power spectrum. This strong AE signal corresponding to fracture initiation was of 70 dB amplitude and 350 kHz average frequency.

In the CVN test, fracture initiation occurred within a very short time period, and the high-speed camera cannot be installed to observe the fracture behavior of the specimen. Therefore, it is impossible to determine directly the location of fracture initiation in the CVN

load-displacement curve. **Figure 20** shows the results of the CVN tests at room temperature. It can be seen that there are some strong signals before the peak load, marked in red in **Figure 21**. It is evident that these signals related with crack initiation with approximately 10% error.

4. Conclusions

In this chapter, the acoustic emission (AE) monitoring has been shown to accurately reflect the start of plastic deformation, initiation of fracture, and fracture mode (ductile or brittle) during tensile, three-point bend impact, and testing of steels. The AE signal density, amplitude, and frequency could vary by 2–3 times with occurrence of those phenomena. The dependences of absolute values of AE signal parameters on test temperature, loading rate, sample geometry, and fracture mode have been obtained and analyzed. The effect of material chemistry and microstructure on AE activity during testing requires more detailed investigation.

For single edge-notched tension test:

- The AE monitoring technique was used for the first time during the SENT test of X70 and X80 line pipe steels. AE activity started before the yield point, due to the stress concentration at the crack tip and increased before the maximum load was reached, due to the fracture initiation. Toward the end of the test, the AE hit density increased, due to the multiple fracture;

- With an increase in strain rate, the AE activity increased.

- The fracture initiation point can be detected by a sudden change in the AE activity. The fracture initiation in the studied steel was marked by the AE signal with 65–75 dB amplitude and a 300–350 kHz average frequency prior to the maximum load point.

For Charpy V-notch test:

- With test temperature decreasing the average frequency of the burst-type AE signals increased. The ductile-to-brittle transition temperature (DBTT) was found to be in the range of −60 to −80°C for the tested steel. A sudden drop in the load observed at −60°C occurred due to the brittle fracture and generated a 350 kHz average frequency burst-type AE signal;

- Charpy specimens with various thicknesses were tested for the first time using the AE monitoring technique. With a decrease in specimen thickness from 10 to 5 mm, the AE average frequency decreased from 150 to 50 kHz;

- It was impossible to observe directly the fracture initiation in the CVN test. The quasi-static three-point bending tests using the same specimens were carried out. The fracture initiated before the peak load was reached. In the CVN tests, strong AE signals were observed before the peak load, and these are believed to correspond to fracture initiation;

- The fracture mode during impact testing can be predicted using AE waveform and power spectra methodologies. In this work, 50–200 kHz frequency signals corresponded to ductile fracture and 250–350 kHz frequency signals corresponded to brittle fracture.

Acknowledgements

Author details

Turbadrakh Chuluunbat[1]* and Andrii Kostryzhev[2]

*Address all correspondence to: turbadrakh@mandakh.mn

1 Department of Science and Engineering, Mandakh University, Ulaanbaatar, Mongolia

2 School of Mechanical, Materials, Mechatronic and Biomedical Engineering, University of Wollongong, Australia

References

[1]   Miller RK. Acoustic Emission Testing. The McGraw-Hill Companies; 2003

[2]   Gross CU, Ohtsu M. Acoustic Emission Testing. Heidelberg, Berlin: Springer; 2008

[3]   Muravin B, Carlos MF. Guide for development of acoustic emission application for examination of metal structure. Journal of Acoustic Emission. 2011;**29**:142-148

[4]   Kostryzhev AG. Detection of crack growth in rail steel using acoustic emission. Ironmaking and Steelmaking. 2012;**2**:1-6

[5]   Wevers M. Listening to the sound of materials: Acoustic emission for the analysis of material behavior. NDT and E International. 1997;**30**:99-106

[6]   Hellier C. Handbook of Nondestructive Evaluation. New York, London: McGraw-Hill; 2001

[7]   Ingham T. Acoustic emission characteristics of steels part 1: Acoustic measurements from tensile tests. International Journal of Pressure Vessels and Piping. 1974;**2**:31-50

[8]   Vallen H. Acoustic Emission Testing Fundamentals, Equipment, Applications. The e-Journal of Nondestructive Testing. 2002;**7**:9-10

[9]   Dunegan HL. Factors affecting acoustic emission response from materials. ASTM Acoustic Emission Standards. 1972;**2**:100-113

[10] Tonolini F. General review of developments in acoustic emission methods. International Journal of Pressure Vessels and Piping. 1987;**28**:179-201

[11] Crutzen S. Developments in fracture mechanics and non-destructive examination. Nuclear Engineering and Design. 1992;**134**:59-86

[12] Kostryzhev AG. Acoustic emission monitoring of split formation during Charpy impact testing of high strength steel. Materials Science and Technology. 2012;**28**:240-242

[13] Ono K. Current understanding of mechanisms of acoustic emission. Journal of Strain Analysis for Engineering Design. 2005;**40**:1-15

[14] Muravin B. Acoustic emission science and technology. Journal of Building and Infrastructure Engineering of the Israeli Association of Engineers and Architects. 2009;**1**:4-5

[15] Eitzen DG, Wadley HNG. Acoustic emission: Establishing the fundamentals. Journal of Research of the National Bureau of Standards. 1984;**89**:75-100

[16] Frederick JR, Felbeck DK. Dislocation motion as a source of acoustic emission. ASTM Acoustic Emission Standards. 1972;**78**:129-139

[17] Carpenter SH, Higgins FP. Sources of acoustic emission generated during the plastic deformation of 7075 aluminum alloy. Metallurgical Transactions A. 1977;**8**:1629-1632

[18] Barat K. Low temperature tensile deformation and acoustic emission signal characteristics of AISI 304LN stainless steel. Materials Science and Engineering A. 2013;**597**:37-45

[19] Roberts TM. Acoustic emission monitoring of fatigue crack propagation. Journal of Constructional Steel Research. 2003;**59**:695-712

[20] Mukhopadhyay CK. Study of tensile deformation behaviour of M250 grade maraging steel using acoustic emission. Journal of Materials Science. 2010;**45**:1371-1384

[21] Mukhopadhyay CK. The influence of notch on the acoustic emission generated during tensile testing of nuclear grade AISI type 304 stainless steel. Materials Science and Engineering A. 2000;**276**:83-90

[22] Kral Z. Crack propagation analysis using acoustic emission sensors for structural health monitoring systems. Scientific World Journal. 2013;**2013**:1-4

[23] Han Z. Effects of strain rate and notch on acoustic emission during the tensile deformation of a discontinuous yielding material. Materials Science and Engineering A. 2011;**528**:4372-4380

[24] Blanchette Y, Dickson JI. Acoustic emission behaviour during crack growth of 7075-T651 AI alloy. Engineering Fracture Mechanics. 1986;**24**:647-656

[25] Fallahi A. Monitoring of the deformation and fracture process of dual phase steels employing acoustic emission techniques. Materials Science and Engineering A. 2012;**548**:183-188

[26] Ohtsu M, Ono K. AE source location and orientation determination of tensile cracks from surface observation. International Nondestructive Testing. 1988;**21**:143-150

[27] Roy H. Acoustic emissions during fracture toughness tests of steels exhibiting varying ductility. Materials Science and Engineering A. 2008;**486**:562-571

[28] Clark G, Knott JF. Acoustic emission and ductile crack growth in pressure-vessel steels. Metal Science. 1977;**6**:531-536

[29] Wadley HNG. Acoustic emission for physical examination of metals. International Metals Reviews. 1980;**2**:41-64

[30] Mostafavi S. Acoustic emission methodology to evaluate the fracture toughness in heat treated AISI D2 tool steel. Journal of Materials Engineering and Performance. 2011;**21**:2103-2116

[31] Chuluunbat T, Koztryzhev AG. Influence of loading conditions during tensile testing on acoustic emission. Key Engineering Materials. 2014;**626**:121-126

[32] Mukhopadhyay CK. Acoustic emission during fracture toughness tests of SA333 Gr.6 steel. Engineering Fracture Mechanics. 2012;**96**:294-306

[33] Yusof MFM. Acoustic emission behavior during fatigue crack of API5LX70 gas pipeline steel. Applied Mechanics and Materials. 2011;**80**:148-152

[34] Richter H. The use of acoustic emission to determine characteristic dynamic strength and toughness properties of steel. Nuclear Engineering and Design. 1999;**188**:241-254

[35] Tronskar JP. Application of acoustic emission for measuring crack initiation toughness in instrumented Charpy impact testing. Journal of Testing and Evaluation. 2003;**31**:222-233

[36] Fearnehough GD. Fracture propagation control in gas pipelines: A survey of relevant studies. International Journal of Pressure Vessels and Piping. 1974;**2**:257-282. DOI: 10.1016/0308-0161(74)90007-6

[37] Rivalin F. Ductile tearing of pipeline steel wide plates I. Dynamic and quasi-static experiments. Engineering Fracture Mechanics. 2001;**68**

[38] Cravero S, Ruggieri C. Correlation of fracture behavior in high pressure pipeline with axial flaws using constraint designed test specimens-Part 1: Plane-strain analysis. Engineering Fracture Mechanics. 2005;**72**:1344-1360

[39] DNV-P-F108. Fracture Control for Pipeline Installation Methods: Introducing Cyclic Plastic Strain. Norway: Det Norske Veritas; 2006

[40] Australian-Standard-1544.2. Method for Impact Tests on Metals. Part 2: Charpy V-Notch. Sydney: Standards Australia International Ltd.; 2003